Mon. Not. R. Astron. Soc. **265**, 316–328 (1993)

Simulation of the X-ray light curves of intermediate polars

A. J. Norton
Department of Physics, The Open University, Walton Hall, Milton Keynes MK7 6AA

Accepted 1993 May 14. Received 1993 April 8; in original form 1993 January 12

ABSTRACT

A technique is presented for simulation of the X-ray light curves of intermediate polars. The model includes the effects of self-occultation of the emission regions by the body of the white dwarf, and variation of photoelectric absorption and electron scattering as the aspect angles of the emission regions change, and the effect of accretion occurring through a disc, directly via the accretion stream or by a combination of both. Both the variation of the rate of accretion on to a given emission region and its effective 'migration' around the magnetic pole are taken into account. These features naturally arise in a system that is fed (at least in part) directly by the stream. Results are considered for two specific emission-region geometries, namely a filled circle and a semicircular arc, over a wide range of parameter space in each case. Disc-fed, non-accretion disc and discless accretion are each considered, both in the low and high X-ray energy regime and at a range of inclination angles and magnetic axis offset angles. The main conclusion of this work is that very complex pulse profiles can result from innately symmetrical geometrical and physical situations. The results obtained in the case of discless accretion feeding arc-shaped emission regions are compared with recent observational data and shown to produce qualitatively similar profiles. Finally, ways are considered in which this simple approach may be extended to include a more realistic description of the conditions that exist in intermediate polars.

Key words: accretion, accretion discs – binaries: close – stars: magnetic fields – novae, cataclysmic variables – white dwarfs – X-rays: stars.

1 INTRODUCTION

Intermediate polars are semidetached, interacting binary systems containing a late-type, Roche-lobe-filling, dwarf star and a strongly magnetic white dwarf. Accretion on to the white dwarf is controlled by its magnetic field, such that the flow is channelled towards the magnetic polar regions where it is decelerated. X-rays are emitted from the settling region between the shock and the white dwarf surface. The magnetic axis and spin axis of the white dwarf are presumed to be misaligned such that the emission that is seen from regions in the vicinity of the magnetic poles is modulated at the rotation period of the white dwarf. This X-ray pulsation, with periods of the order of a few hundred seconds, is the defining characteristic of an intermediate polar.

In fact, the X-ray emission from these systems is modulated in a complex way, and shows variations at the spin period of the white dwarf, usually at the binary period of the system, and often at one or more 'beat' periods as well. Some of the modulations are seen to be energy-independent, whilst others show evidence for phase-varying photoelectric absorption. The highest signal-to-noise ratio X-ray data available for intermediate polars come from the recent *Ginga* observations of EX Hya, FO Aqr, BG CMi, GK Per and RE 0751 + 14, discussion of which individually may be found in Rosen et al. (1991), Norton et al. (1992a,b), Ishida et al. (1992) and Mason et al. (1992) respectively. A summary of all the *Ginga* observations of magnetic cataclysmic variables is given by Ishida (1991). For summaries of the earlier *EXOSAT* observations of intermediate polars, see Norton & Watson (1989) and Hellier, Garlick & Mason (1993), and references therein.

The exact structure of the X-ray light curve is determined to a great extent by the method of accretion on to the magnetic white dwarf, and this has long been a matter of debate. In particular, recent discussion has centred around whether or not accretion occurs via a disc or directly from the accretion stream as in polars (see King & Lasota 1991; Hellier 1991, 1992; Norton et al. 1992a,b). A third possibility, known as a non-accretion disc, allows for a disc to be pre-

sent, but all, or part of, the accretion flow skims over the faces of the disc before interacting with the magnetosphere (King & Lasota 1991, and references therein). In this work, 'non-accretion disc' will be used to describe a system in which both disc-fed and stream-fed accretion occur simultaneously. Schematic diagrams for each of these scenarios are illustrated in Figs 1(b)–(d), along with (for completeness) the case of accretion in a non-magnetic system (Fig. 1a).

Wynn & King (1992) recently presented a set of theoretical X-ray power spectra of intermediate polars with various accretion geometries. They concentrated on the presence (or otherwise) of beat frequency effects in their results, as a diagnostic of disc-fed or stream-fed accretion. This paper follows a similar approach, but instead concentrates on the pulse profiles and other modulation shapes generated by such models. Hitherto, little attempt has been made to simulate the X-ray light curves of intermediate polars by taking into account geometrical, absorption/scattering and accretion effects. The aims of this work are to present an outline of such a technique, and so predict the spin- and beat-pulse profiles and orbital modulation that will be seen in a variety of simple cases.

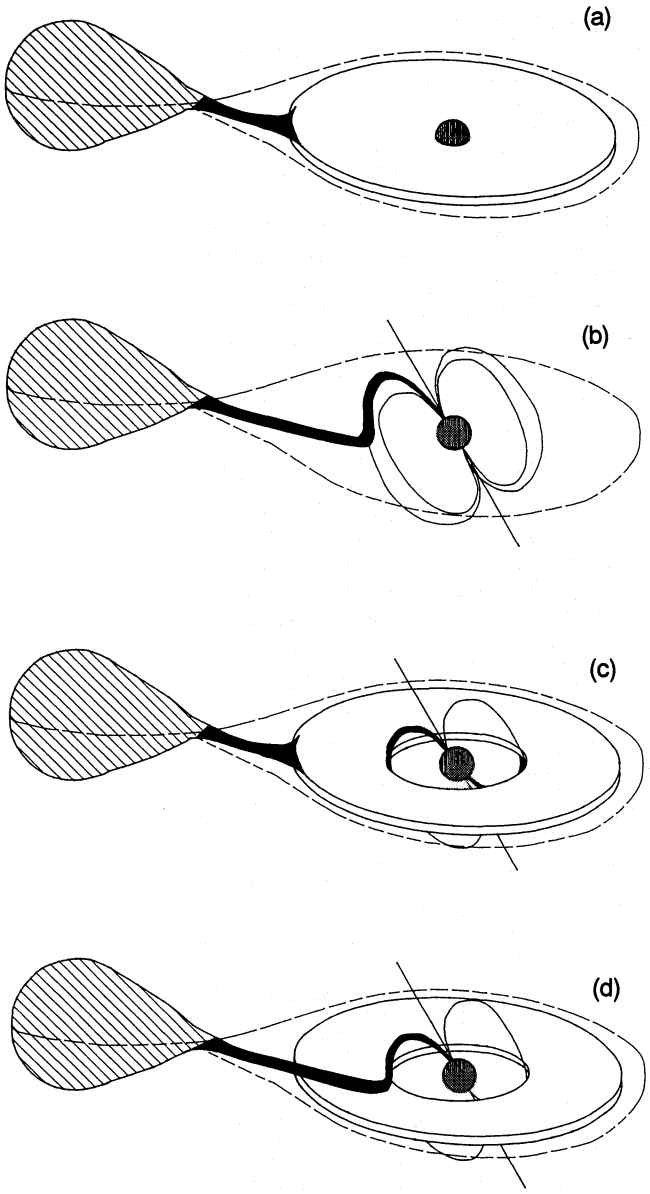

Figure 1. Schematic diagrams of accretion in cataclysmic variables. (a) Non-magnetic CV with no disruption of the accretion disc. (b) Stream-fed magnetic CV in which the formation of an accretion disc is prevented. (c) Disc-fed magnetic CV in which the accretion disc is disrupted at the magnetosphere boundary. (d) Magnetic CV with non-accretion disc in which a disrupted disc exists, but in which (some of) the accreting material skims over the surface to impact the magnetosphere directly as in (b).

2 ACCRETION ON TO A MAGNETIC WHITE DWARF

As indicated above, many factors influence the temporal variation in the X-ray signal that is observed from intermediate polars. These factors may be broadly characterized as falling into the five general areas discussed below. Note that the technique discussed here applies only to *X-ray* light curves, or effects produced by direct accretion on to the white dwarf. The arguments here will not necessarily apply to the optical modulations that are seen from intermediate polars.

2.1 Geometry of the accretion regions

The observed X-ray emission will depend on the number of accretion/emission regions that are present, their size and shape, their location on the white dwarf and their relative activity. It is usually assumed that one or both magnetic poles can be sites of accretion, with the accretion occurring over a region determined by the 'footprint' on the white dwarf surface of the magnetic field lines to which the material initially attached at the magnetosphere. Hence the location is largely determined by the offset angle between the magnetic axis and the spin axis of the white dwarf, assuming a dipole magnetic field. Various geometries have been suggested for these accretion regions (also known as 'polecaps'), including filled circles, annuli, arcs or crescents. The area of these regions has been taken to be anything between 0.01 and 10 per cent of the surface area of the white dwarf, and the emission is generally assumed to arise very close to the white dwarf surface (but see Section 5). The accretion region around the magnetic pole located above the orbital plane of the system will be referred to as the 'upper' magnetic pole, and the one that is below the orbital plane will be referred to as the 'lower' magnetic pole.

2.2 Self-occultation

As the white dwarf rotates, different fractions of each accretion region will become occulted by the body of the white dwarf. The fraction occulted will depend on the parameters discussed above, and also on the inclination angle between the line of sight and the orbital plane of the system. This effect alone can give rise to pulse profiles which are independent of X-ray energy (as long as an asymmetry exists between the visibility of the two polecaps or between their properties). The variety of pulse profiles that are possible, simply as a result of the occultation of a single circular emission region, was discussed by King & Shaviv (1984) in the

first attempt to understand the X-ray light curves of intermediate polars.

2.3 Local photoelectric absorption/electron scattering

The optical depths due to local photoelectric absorption and electron scattering in the accreting material immediately above the magnetic poles will usually vary between lines of sight directed horizontally across the accretion regions and lines of sight directed vertically on to the accretion regions (King & Shaviv 1984). Hence, as the white dwarf rotates, presenting each accretion region at a varying aspect angle, so the relative attenuation of the X-ray flux will vary, thus giving a modulated signal. In the basic model presented by King & Shaviv, the difference between these 'edge-on' and 'face-on' optical depths is such that minimum attenuation occurs when a given pole is seen from the side, and maximum attenuation when it is seen from above, for all but the largest accretion regions (see Section 3).

2.4 Accretion controlled by the magnetic field

In a disc-fed system, the accretion flow passes through a disc which is disrupted at the white dwarf magnetosphere, whereupon the material attaches to the magnetic field lines and is channelled towards the poles (Fig. 1c). Hence the accretion is presumed to be azimuthally symmetric and flows more or less equally on to *both* magnetic poles of the white dwarf at *all* phases. By contrast, in a stream-fed system (Fig. 1b), the accretion stream impacts the magnetosphere directly. Accretion is therefore presumed to be confined to a narrow azimuthal range and may be channelled predominantly on to a *single* pole at any instant. In phase-locked polars this means that the accretion pattern remains constant. In intermediate polars, however, the balance of the accretion flow will effectively flip between the two poles every half a beat cycle, as the white dwarf rotates with respect to the orbital frame. The effect of this will be to cause a different pattern of accretion as a function of spin phase at different points in the binary orbit. This will be seen as an orbital dependence of the spin pulse or as a beat frequency in the X-ray power spectrum. In the non-accretion disc scenario (Fig. 1d), the assumption made in this work is that a *combination* of disc-fed and stream-fed accretion occurs simultaneously, so giving rise to both phase-independent and phase-dependent patterns of accretion on to the white dwarf.

2.5 Orbital phase modulation

It is also possible that material in the accretion stream introduces an additional column density when it lies between the observer and the white dwarf. This could happen regardless of the presence or nature of an accretion disc. However, in the case of discless or non-accretion disc models, the stream impact with the magnetosphere is thought to give rise to a 'splash' of material, so producing an extended region of local photoelectric absorption and electron scattering (Hameury, King & Lasota 1986). The extra attenuation introduced will not alter the pulse profile shape, but will change the relative modulation depth as a function of orbital phase and introduce an explicit orbital modulation.

2.6 Relative phasing of pulsations

The three effects that can actually cause a pulsed X-ray signal (whether at the spin or beat period) are therefore self-occultation by the white dwarf, the variation between face-on/edge-on optical depths and the variation in the local accretion rate caused by the stream flipping between the two poles. With plausible values for system inclination and magnetic axis offset angles, the upper magnetic pole will always be the dominant source of emission. Furthermore, unless the emission regions are very large, occultation and photoelectric absorption/electron scattering will always act in *anti-phase* with each other for this upper pole – i.e. as the emission region disappears over the rim of the white dwarf, it is seen progressively from the side and hence through a lower optical depth. By contrast, the stream flipping effect will act in phase with the occultation effect when the stream lies between the observer and the white dwarf, and in phase with the absorption/scattering effect when the stream is on the far side of the white dwarf. To appreciate this more clearly, note that when the upper pole is least occulted it will be predominantly fed if the stream lies between the observer and the white dwarf. Conversely, when the upper pole is most occulted, it will be predominantly fed when the stream lies on the far side of the white dwarf. This reflects the fact that the variation in stream feeding is a beat-period effect and relies on the orientation of the white dwarf with respect to the orbital frame, not the observer's frame of reference.

3 IMPLEMENTATION OF THE SIMULATION

In an attempt to simulate the X-ray light curves of intermediate polars, a computer code has been written that incorporates the features described above. In this general model, spin phase zero ($\phi_{\rm spin}=0.0$) is defined to correspond to the position at which the upper magnetic pole points towards the observer and the surrounding emission region is seen most nearly face-on. Spin phase 0.5 therefore corresponds to the phase at which the emission region around the upper magnetic pole is at its greatest obscuration around the far side of the white dwarf. X-ray orbital phase zero ($\phi_{\rm orb}=0.0$) is defined to be the phase at which the accretion stream is on the far side of the white dwarf, i.e. the companion star is near superior conjunction. At orbital phase 0.5, the accretion stream (and companion star) lies between the observer and the white dwarf.

3.1 Parametrization

Within this general framework, the mode of accretion is described using the following parameters.

i: the inclination angle of the binary system with respect to the observer's line of sight. $i=90°$ describes an edge-on system; $i=0°$ describes a face-on system.

$m(n)$: the angle between the spin axis and the magnetic axis for each of the n accretion regions, assuming the regions to be centred around the magnetic poles. For a dipole magnetic field, obviously, $m(2)=m(1)+180°$.

$f(n)$: the fraction of the white dwarf surface area covered by each accretion region, assuming that each is represented by a filled circle. Hence f describes the area of the *envelope*

containing the accretion region whose shape is further defined by the parameters f' and f''.

$f'(n)$: each accretion region is divided into a number of circular rings, and each of these into a number of sectors, where each sector is typically 10^{-5} of the area of the white dwarf. This parameter describes what fraction of the rings comprising a given region are accreting/emitting. For example, $f'=0.1$ describes an annulus whose thickness is 10 per cent of the radius of the circle described by f.

$f''(n)$: the fraction of sectors within each ring that are emitting/accreting. Hence $f''=1.0$ describes a circle; $f''=0.5$ describes a semicircle. By using combinations of f' and f'', various geometries can be ascribed to each accretion region. The actual area, $\mathcal{F}$, of each accretion region as a fraction of the total white dwarf surface area is therefore calculated as

$$\mathcal{F}=ff'f''(2-f'). \tag{1}$$

$\psi(n)$: this parameter is only relevant if $f''(n)<1$, and it describes the angle of the centre of distribution of sectors in any ring with respect to the line between the spin pole and magnetic pole of the white dwarf. For example, if the accretion region has an arc-like geometry and if $\psi=0°$, then the centre of the arc, the magnetic pole and the spin pole lie along a great circle on the white dwarf surface, in that order. If $\psi=180°$, then the centre of the arc lies between the magnetic axis and the spin axis, but once again along a great circle. (Note that this assumes that $m>0°$, i.e. that the magnetic pole is offset from the spin pole.)

E: the X-ray energy (in keV) of the simulated light curve that is produced. This affects the photoelectric absorption terms that contribute to the modulation.

δ: a parameter representing the maximum fraction of the accreting material that can accrete on to any one pole at any instant. The parameter is constrained within the range $0.5\leq\delta\leq1.0$, and hence the 'baseline accretion' or minimum fraction that accretes on to each pole is defined as $1-\delta$. The fraction available to flip between the poles as the white dwarf rotates is therefore $2\delta-1$. It can be seen that disc-fed accretion is represented by the value $\delta=0.5$, whereby each pole receives exactly half the accreting material all the time. Stream-fed accretion is represented by the value $\delta=1.0$, such that the accretion rate on to each pole varies between zero and 100 per cent of the total available. Intermediate values of δ may be taken to represent various cases of non-accretion disc behaviour in which both stream-fed and disc-fed accretion take place. For example, if $\delta=0.7$, then 60 per cent of the material accretes through the disc, 30 per cent on to each pole. The remaining 40 per cent of the material accretes through the stream such that the 'disc plus stream' accretion rate on to each pole varies between 30 and 70 per cent of the total accreting material.

Two additional parameters which can be used to characterize the effects described in Section 2, but are effectively not used in the examples discussed later, are described below for completeness.

$S_{act}(n)$: the relative 'activity' of each emission region allows 'hotspots' to be described as separate regions. In the simplest case (as used later), $S_{act}(1)=S_{act}(2)=1$, and both poles are equally active.

N_H: the maximum column density due to the accretion stream when it lies directly between the observer and the emission regions. The attenuation caused by this is assumed to be effective only over the orbital phase range $0.25\leq\phi_{orb}\leq0.75$, and is represented by

$$A_{orb}\simeq\exp[(E^{-3.0}+0.0067)\,N_H\cos(2\pi\phi_{orb})], \tag{2}$$

where N_H is in units of 10^{22} atoms cm^{-2}. In the examples discussed later, this parameter was set to zero, i.e. no explicit orbital-dependent photoelectric absorption or electron scattering was introduced.

3.2 Instantaneous accretion rates

In those cases for which some fraction of the accretion occurs directly via the stream (i.e. $\delta>0.5$), the instantaneous accretion rate on to a given pole, $S_{accr}(n)$, will depend on the parameter δ and the angular distance, $\alpha(n)$, between the magnetic pole and the site at which the accretion stream impacts the magnetosphere. It is likely that the majority of the accretion flow will be directed towards the magnetic pole that is 'closest' to the impact site at any instant. However, it is unlikely that *all* the accretion flow will be so diverted, and in certain cases, for instance if $m(1)=0°$ and $m(2)=180°$, the accretion is unlikely to have a preferred direction of flow. Bearing in mind the definitions of orbital and spin phase zeros mentioned earlier, the angular distance between each magnetic pole and the accretion-stream impact site may be expressed as

$$\cos\alpha(n)=-\sin m(n)\cos2\pi(\phi_{spin}-\phi_{orb}) \tag{3}$$

(assuming that the stream is generally confined to the orbital plane prior to impact with the magnetosphere). The instantaneous accretion rate on to a given magnetic pole is presumed to vary in proportion to this angle. In particular, a cosine weighting is assumed, and the accretion rate calculated as

$$S_{accr}(n)=(1-\delta)+(2\delta-1)\left[\frac{\cos\alpha(n)+1}{\cos\alpha(1)+\cos\alpha(2)+2}\right]. \tag{4}$$

In this equation, the first term represents the disc-fed fraction of the accretion flow, and the second term represents the stream-fed fraction. For a dipole magnetic field, $\alpha(2)=\alpha(1)+180°$, but the above equation also allows for the effects of an offset dipole, for instance, whilst still maintaining $S_{accr}(1)+S_{accr}(2)=1$, i.e. a constant total accretion rate. Note that this weighting is somewhat arbitrary, but it does exhibit the general property of a dependence on $(\phi_{spin}-\phi_{orb})$ which will undoubtedly occur. Hence the stream-fed accretion rate on to each polar cap varies smoothly with the 'beat phase' of the system.

3.3 Accretion-region migration

An important point to realize is that, if an accretion region is fuelled directly by the accretion stream (i.e. $\delta>0.5$), and if the accretion region has a non-circular geometry (i.e. $f''<1.0$), then the accretion region will effectively 'migrate' around the magnetic pole to follow the incoming accretion stream. The effect of this is a variation in the angle ψ as a function of orbital and spin phase. For such stream-fed accretion regions, the effective position (ψ_{eff}) of the centre of

distribution of the sectors making up the polar cap is given by

$$\psi_{\rm eff}(n) = \psi(n) + 2\pi(\phi_{\rm spin} - \phi_{\rm orb} + 0.5). \quad (5)$$

Hence, in the case of a non-accretion disc scenario ($0.5 < \delta < 1.0$), each of the upper and lower accretion regions on the white dwarf can be considered as the sum of two components: one is fixed on the white dwarf and is fed from the disc, and one moves around the magnetic pole and is fed from the stream. In the cases considered here, it is assumed, for simplicity, that each component of the accretion region at a given pole has the same shape and size. In the extreme disc-fed ($\delta = 0.5$) and stream-fed ($\delta = 1.0$) situations, only one component at each pole will be present.

3.4 Face-on/edge-on absorption and scattering

The local attenuation, $A_{\rm aspect}$, for a particular sector in a given accretion region is calculated using the optical depths due to photoelectric absorption and electron scattering when looking across the accretion region ($\tau_{\rm h}$) and when looking vertically down on to the accretion region ($\tau_{\rm v}$). These in turn are approximated by the following equations, derived from those given by King & Shaviv (1984). Assuming that the photoelectric and electron scattering optical depths, τ(pe) and τ(es), are related by

$$\tau({\rm pe}) \simeq 600\,\tau({\rm es})\,E^{-3.0}, \quad (6)$$

where E is in keV, the total optical depth, τ(pe) + τ(es), in each direction is

$$\tau_{\rm h} \simeq (8.1E^{-3.0} + 0.014)\,S_{\rm accr}\mathscr{F}^{-0.5}, \quad (7)$$

$$\tau_{\rm v} \simeq (2.4E^{-3.0} + 0.004)\,S_{\rm accr}\mathscr{F}^{-1.0}, \quad (8)$$

assuming a total accretion rate of 10^{17} g s^{-1}, a white dwarf mass of 1 $M_\odot$ and a white dwarf radius of 0.55×10^9 cm, as determined using the mass–radius relationship of Nauenberg (1972). Note that $\tau_{\rm v} > \tau_{\rm h}$ unless $\mathscr{F}$ is very large, the limiting value for the accreting area being ~9 per cent of the surface area of the white dwarf. Hence minimum attenuation of the X-ray flux will generally be observed when an accretion region is viewed from the side, as noted earlier.

If θ is the angle that the normal vector to a given sector makes with respect to the line of sight, then $\theta = 0°$ corresponds to a face-on view, and $\theta = 90°$ corresponds to an edge-on view of a particular sector in an accretion region. The attenuation factor due to this aspect-angle effect is therefore calculated as

$$A_{\rm aspect} = \exp[-(\tau_{\rm h}\sin^2\theta + \tau_{\rm v}\cos^2\theta)] \quad (9)$$

for each sector.

3.5 Generation of a light curve

Having described the physical situation using the parameters listed above, a light curve is then generated as follows. At a given time-step, the relative spin phase and orbital phase are determined. The position of each sector, in each ring, in each accretion region is calculated and projected on to a plane perpendicular to the line of sight. It is then determined whether the sector in question is visible or whether it is occulted by the body of the white dwarf. If visible, the relative flux per sector ($S_{\rm act}$) is multiplied by the local accretion rate ($S_{\rm accr}$), the attenuation due to the accretion stream ($A_{\rm orb}$) and the attenuation due to the aspect angle of the sector with respect to the line of sight ($A_{\rm aspect}$). Note that the factor $S_{\rm accr}$ is composed of two terms representing the disc-fed accretion rate and the stream-fed accretion rate at each pole. Only the relevant term is applied to each component of each accretion region.

The contributions from all visible sectors are accumulated in this way, building up a measure of the total flux, I, at a particular spin phase of the white dwarf and orbital phase of the system:

$$I(\phi_{\rm spin}, \phi_{\rm orb}) = \sum_{\rm sectors} S_{\rm act}S_{\rm accr}A_{\rm orb}A_{\rm aspect}. \quad (10)$$

A light curve is thus generated spanning typically five orbital cycles and 80 spin cycles of the white dwarf, using ~10^4 time-bins. (These parameters are chosen to be characteristic of the coverage obtained in a single *Ginga* observation of an intermediate polar.) The maximum flux of the light curve is normalized to a value of unity to enable comparison between the various models. This resulting time series is then folded at the input spin period and orbital period, and also at the calculated beat period, where $1/P_{\rm beat} = 1/P_{\rm spin} - 1/P_{\rm orb}$. Finally, folds at the spin period in two mutually exclusive ranges of orbital phase ($\phi_{\rm orb} = 0.25$–0.75 and $\phi_{\rm orb} = 0.75$–0.25) are also calculated. Note that the orbital and spin periods used are chosen to be non-integral multiples of each other in order to achieve complete coverage in beat phase.

4 RESULTS

Simulations were carried out for two classes of geometry which have previously been considered as likely descriptions of the white dwarf polar caps, namely filled circles and semi-circular arcs. For each class of geometry, several situations were considered, corresponding to the eight cases shown in Table 1.

Note that cases (i) and (ii) in Table 1 are probably physically unrealistic in that *no* photoelectric absorption or electron scattering is assumed, i.e. the optical depths are set to zero at all times. (Virtually all intermediate polars show evidence for a large local column density.) None the less, these cases provide a starting point for the models as the 'simplest' possible situations in the case of purely disc-fed and purely stream-fed accretion. Also note that, although photoelectric absorption and electron scattering will probably always contribute to the modulation to some extent, at the X-ray energies considered in cases (iii) to (viii), one or the other will be the dominant effect, as shown. These eight cases therefore broadly represent all situations from the simplest disc-fed scenario with no local attenuation to the most complex scenario where self-occultation, photoelectric absorption, electron scattering and a combination of disc-fed and stream-fed accretion all contribute to the X-ray modulation. For each of these eight cases, 16 combinations of i and $m(1)$ were used, where each angle was allowed the values 0°, 30°, 60° and 90°. In all cases, simple dipole fields were assumed, i.e. $m(2) = m(1) + 180°$.

It is important to note that *no asymmetries* are explicitly introduced into any of these models. A dipole symmetry,

Table 1. The range of models simulated.

Case	Dominant Causes of Modulation	Mode of Accretion	Parameter Values E (keV)	δ
i)	Occultation only	Accretion disc	n/a	0.5
ii)	Occultation + Stream feeding	Discless	n/a	1.0
iii)	Occultation + Scattering	Accretion disc	> 20	0.5
iv)	Occultation + Scattering + Stream feeding	Discless	> 20	1.0
v)	Occultation + Scattering + Stream feeding	Non-accretion disc	> 20	0.75
vi)	Occultation + Absorption	Accretion disc	4	0.5
vii)	Occultation + Absorption + Stream Feeding	Discless	4	1.0
viii)	Occultation + Absorption + Stream Feeding	Non-accretion disc	4	0.75

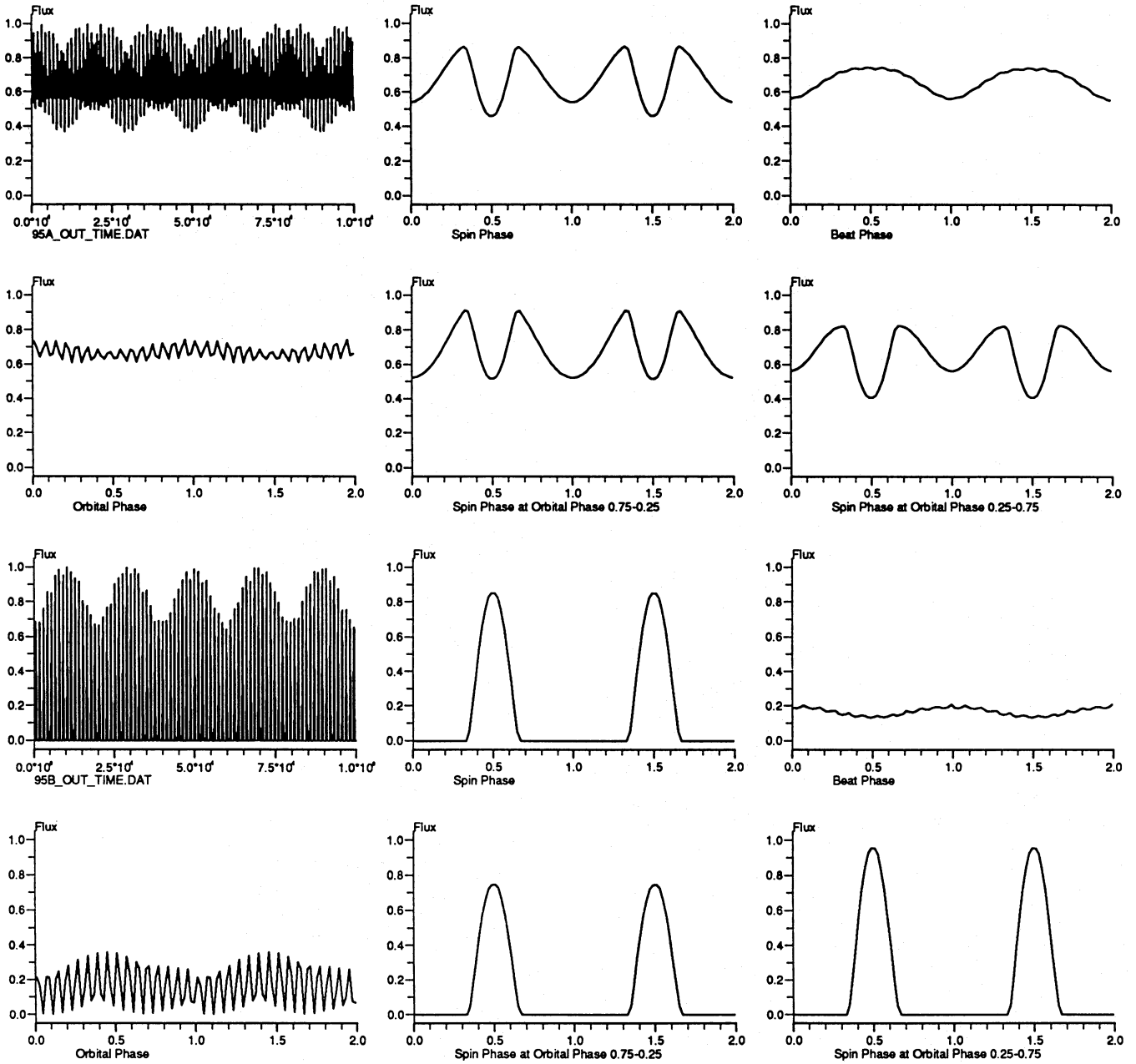

Figure 2. Examples of light curves in the case of circular accretion/emission regions. Input parameters are $i=60°$, $m(1)=30°$, $m(2)=210°$ $f(1)=f(2)=0.01$, $f'(1)=f'(2)=f''(1)=f''(2)=1.0$, $E=4$ and $\delta=0.75$. The first group of six panels represents the light curves that would be generated from the upper pole alone, the second group of six panels represents the output from the lower pole alone, and the final six panels represent the output from both poles. Within each set of six are shown the light curve, the light curve folded at the spin period, folded at the beat period, folded at the orbital period, and folded at the spin period after selection into two mutually exclusive orbital phase ranges. All folds in this and other figures are shown repeated over two cycles for clarity.

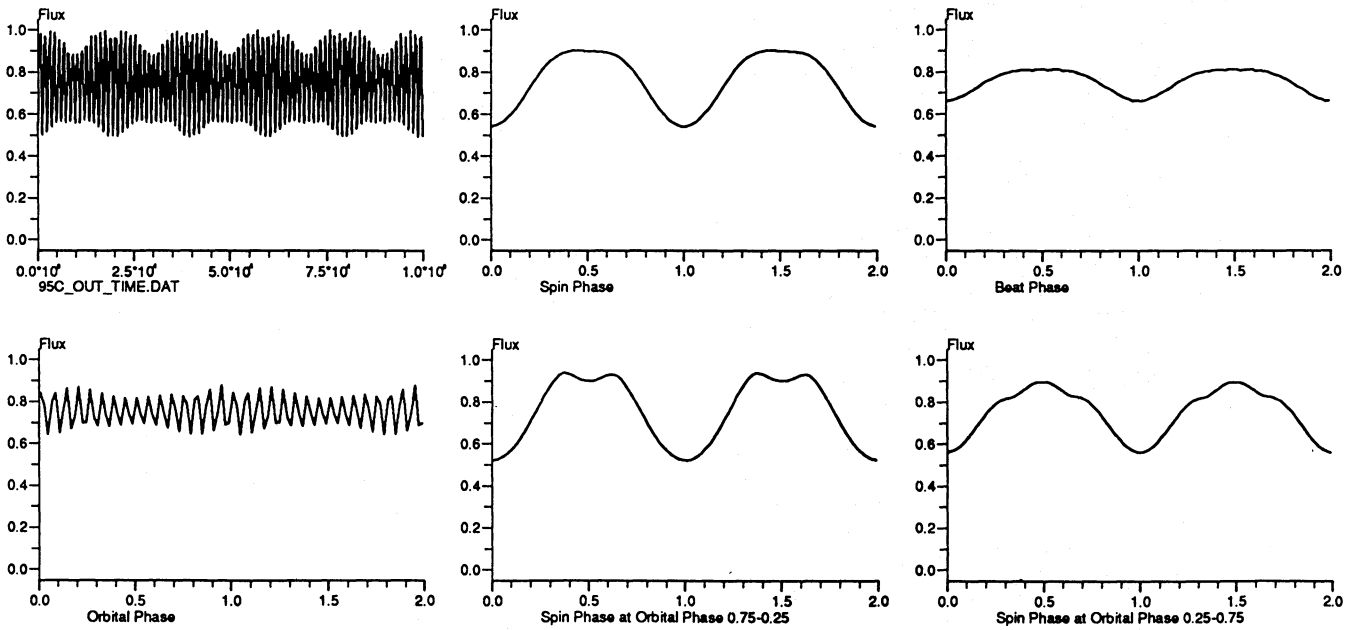

Figure 2 – *continued*

with equally sized/shaped accretion regions around both poles, is assumed in each case, and no special constraints are imposed on the visibility of the lower pole. Nevertheless, because of the effect of stream-fed accretion in particular, highly asymmetric pulse profiles often result.

4.1 Filled-circle geometry

The simplest geometry examined consists of two identical, circular polar caps, each covering 1 per cent of the surface area of the white dwarf [i.e. $f(1)=f(2)=0.01$, $f'(1)=f'(2)=1.0$, $f''(1)=f''(2)=1.0$]. As noted earlier, the parameters S_{act} and N_H were left at 'default' values. Lack of space precludes the printing of all five folded data sets for each of the 128 cases considered for each geometry; moreover, it would be difficult to appreciate any trends from such a presentation. In an attempt to present a simplified description of the results, the following general comments and example light curves should suffice.

When occultation is the only possible cause of modulation, i.e. case (i), light curves folded at the spin, beat and orbital periods all show zero modulation, since an exact cancelling occurs between the visibility of the upper and lower poles. Furthermore, in all the purely disc-fed models, i.e. (i), (iii) and (vi), there is no variation of the spin-fold as a function of orbital phase and zero modulation at the beat and orbital periods, as expected. Beat and orbital modulations are only seen when (at least some of) the accretion occurs directly via the stream, i.e. (ii), (iv), (v), (vii) and (viii). Where a spin or beat modulation is seen, zero modulation when i and/or $m(1)=0°$ tends to transform to a sinusoidal modulation at larger angular values, and into a double-peaked modulation when i and/or $m(1)$ take even larger values approaching 90°. The difference between models at high X-ray energy, i.e. (iii), (iv) and (v), and those at low X-ray energy, i.e. (vi), (vii) and (viii), is that the former tend to have lower modulation amplitudes. This is due to the increasing effect of photoelectric absorption at lower energies. Similarly, the non-accretion disc models, i.e. (v) and (viii), tend to have lower modulation amplitudes than the corresponding purely stream-fed models, i.e. (iv) and (vii).

Fig. 2 contains a light curve and its folded profiles, illustrating an example of the modulation produced in case (viii), when $i=60°$ and $m(1)=30°$. Fig. 3 shows only the spin-folds for a representative set of 16 combinations of the i and $m(1)$ parameters under the constraints of case (viii), i.e. non-accretion disc accretion at low X-ray energy. As noted above, in other cases, i.e. (iii)–(vii), the profile shapes are broadly similar to this, differing only in relative amplitude.

4.2 Arc geometry

This model consists of two identical, semicircular, arc-shaped polar caps, each covering ~0.1 per cent of the surface area of the white dwarf, i.e. $f(1)=f(2)=0.01$, $f'(1)=f'(2)=0.1$, $f''(1)=f''(2)=0.5$. The major difference introduced by the change from filled-circle to arc-shaped polar caps is that the effective migration of the stream-fed component of each polar cap when $\delta>0.5$ is now apparent.

As in the case of the filled-circle geometry, general comments describing the form of modulation together with appropriate examples will have to suffice here. The overall situations where modulation is, and is not, seen are essentially the same ones as in the previous geometry. Also, the previous comments regarding increased or decreased modulation amplitudes between the various cases apply equally here. Where the circular geometry tends to produce 'double sinusoidal' modulations, however, the arc geometry produces rather sharp peaks and troughs in the folded light curves. Also, the polar cap migration referred to above leads to asymmetric notch-like structures, or shoulders, superimposed on underlying sinusoidal modulations whenever the accretion is not purely disc-fed, i.e. in cases (ii), (iv), (v), (vii) and (viii). An example of this is shown in Fig. 4, which con-

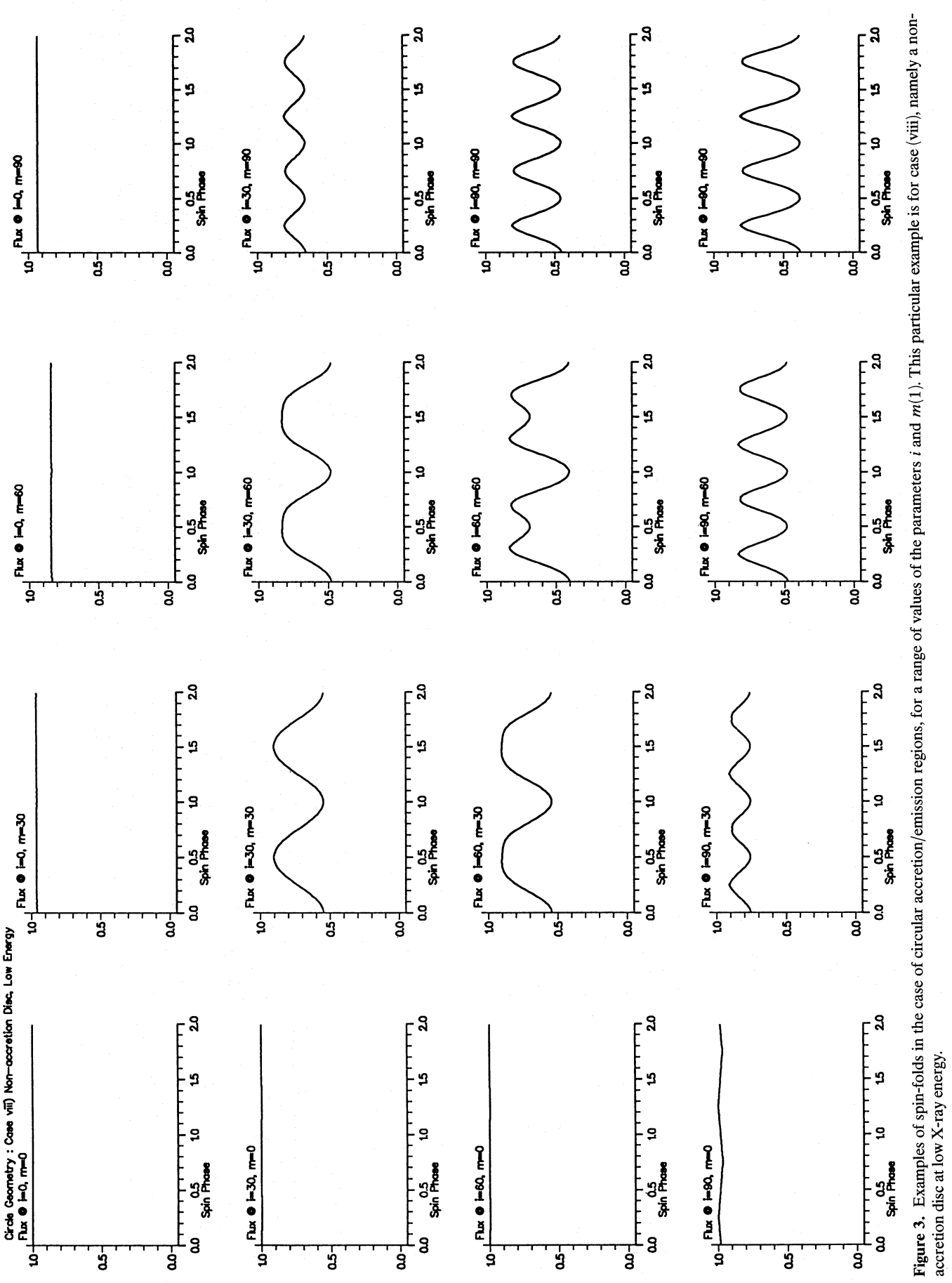

Figure 3. Examples of spin-folds in the case of circular accretion/emission regions, for a range of values of the parameters i and $m(1)$. This particular example is for case (viii), namely a non-accretion disc at low X-ray energy.

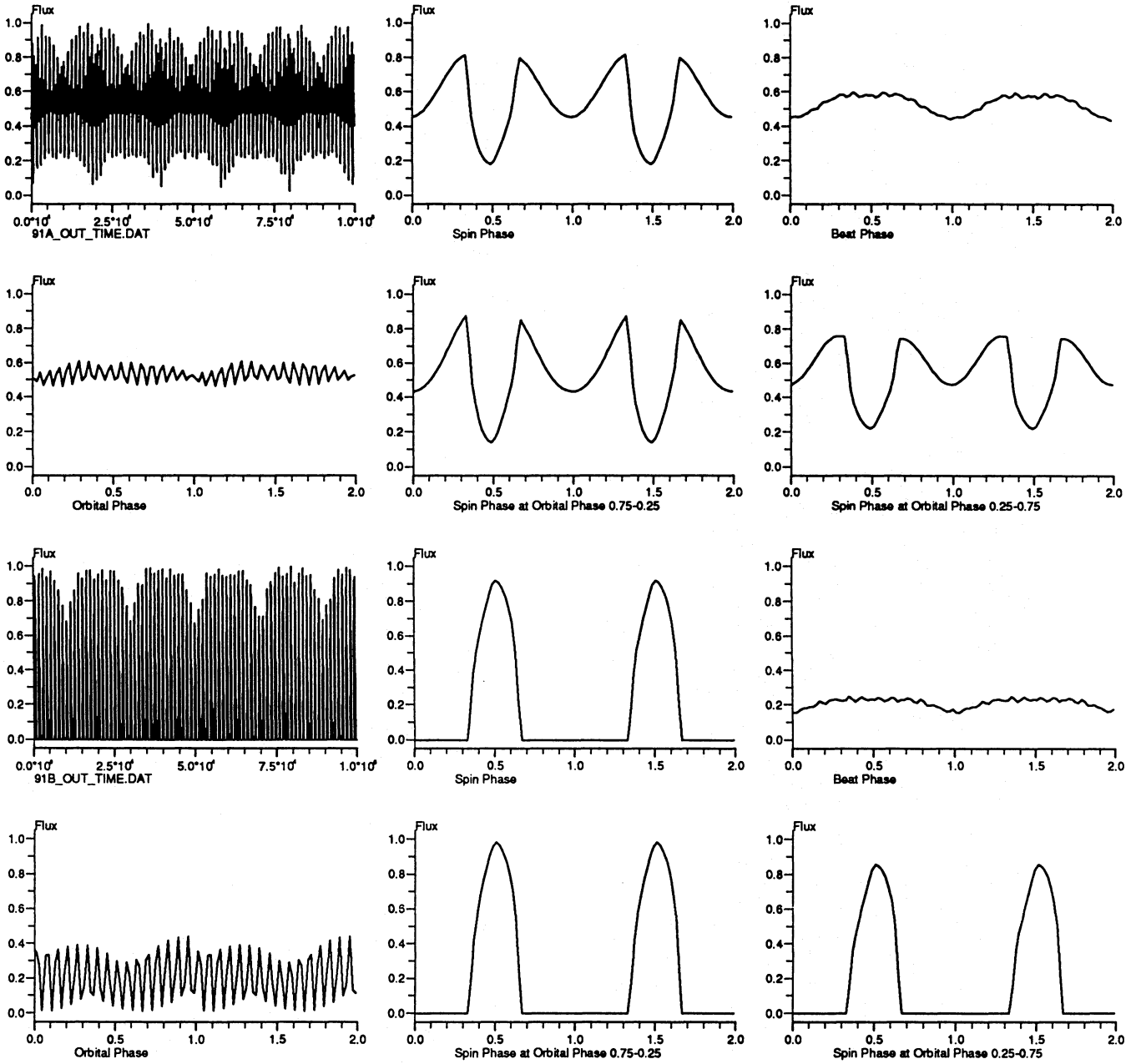

Figure 4. Examples of light curves in the case of arc-shaped accretion/emission regions. Input parameters are: $i=60°$, $m(1)=30°$, $m(2)=210°$, $f(1)=f(2)=0.01$, $f'(1)=f'(2)=0.1$, $f''(1)=f''(2)=0.5$, $E>20$ and $\delta=0.75$. As in Fig. 2, the first group of six panels represents the light curves that would be generated from the upper pole alone, the second group of six panels represents the output from the lower pole alone, and the final six panels represent the output from both poles. Within each set of six are shown the light curve, the light curve folded at the spin period, folded at the beat period, folded at the orbital period, and folded at the spin period after selection into two mutually exclusive orbital phase ranges.

tains the full results from case (v) when $i=60°$ and $m(1)=30°$. Fig. 5 shows only the spin-folds for the full range of i and $m(1)$ parameters for this same non-accretion disc, high X-ray energy case.

4.3 Comparison with observational data

Some of the spin-fold shapes shown in Fig. 5 are remarkably similar to the pulse profiles seen in the *Ginga* data for FO Aqr and BG CMi (Norton et al. 1992a,b), and the *ROSAT XRT* data for RE 0751+14 (Duck et al., in preparation). All these observational data can be interpreted as showing pulse profiles consisting of a 'sinusoidal' component upon which is superimposed a narrow 'notch'.

As an illustration of this similarity, Fig. 6(a) shows the *Ginga* spin-pulse profiles for FO Aqr in four energy bands. Fig. 6(b) shows the results of running the simulation code with the following input parameters: $i=85°$, $m(1)=10°$, $m(2)=190°$, $f(1)=f(2)=0.01$, $f'(1)=f'(2)=0.25$, $f''(1)=f''(2)=0.3$, and $\delta=1.0$. The similarities between the

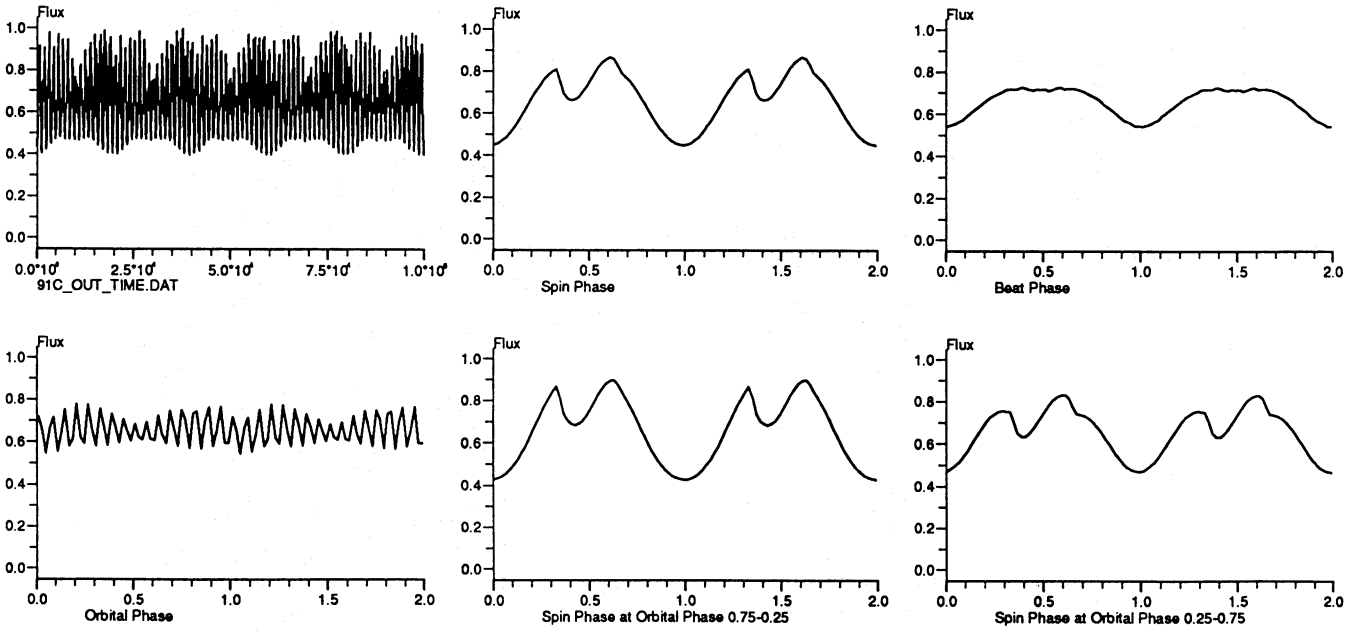

Figure 4 – *continued*

data and the simulation are immediately apparent, especially if a constant-in-phase (or DC) component is added to the simulation at high X-ray energies. Note that there is independent evidence for a high inclination angle in FO Aqr, following the detection of an eclipse using optical spectroscopy (Hellier, Mason & Cropper 1989). However, it must be emphasized that the values used for the set of input parameters that produced these simulated spin-pulse profiles should not be over-interpreted.

First, these simulations assume a very symmetrical geometry: the two accretion/emission regions are identical in size, shape and activity, and are located 180° apart, with no visibility constraints on the lower pole. Secondly, whilst certain parameters are well constrained [i.e. approximate ranges $75° < i < 90°$, $10° < m(1) < 20°$, $0.005 < f < 0.02$] by the necessity to produce spin-pulse profiles of the required shape, other parameters are not. For instance, f' and f'' can take a range of values (≈ 0.1–0.5) and still yield the required 'sinusoid-plus-notch' type of profile; similarly δ is essentially only constrained to be greater than 0.5 (i.e. purely disc-fed accretion is ruled out). This is partly due to the insensitivity of the model to the input parameters, and partly due to the low signal-to-noise ratios of the data. A third point to bear in mind is that a 1-$M_\odot$ white dwarf was assumed with a total accretion rate of 10^{17} g s^{-1}, neither of which values are necessarily correct for FO Aqr. A final caveat is that the simulated pulse profiles are at specific X-ray energies, whereas the real data are accumulated over a range of X-ray energies and modified by the spectral shape of the source and the detector response.

None the less, under the assumptions of this model (i.e. symmetrical, identical accretion regions in a dipole geometry) it is clear that arc-shaped polar caps when fed directly by the accretion stream can broadly reproduce the features seen in the X-ray pulse profiles of FO Aqr and several other intermediate polars. Such a statement is a valuable first step in understanding the X-ray light curves of intermediate polars, despite the limitations mentioned above.

5 DISCUSSION

The major problem in attempting to simulate the X-ray light curves of intermediate polars is the number of free parameters that are necessarily present in the model. Because of this, it is still not possible to obtain unique 'fits' to individual systems in terms of a set of physical parameters. This problem is made worse by the insensitivity of the simulated light curves to certain input parameters. As mentioned earlier, the simulations described in the examples here were for very symmetrical geometries, thereby virtually halving the number of independent input parameters. The inclusion of offset dipoles, different geometries at the upper and lower accretion/emission regions or simply 'hotspots' at certain locations would certainly give rise to a greater range of modulation shapes.

Furthermore, the model described here is undoubtedly still too simplistic, despite the number of free parameters it contains. Improvement of the validity of the model would necessitate the addition of features such as the following.

(1) Emission regions of finite height, with the X-ray emission varying as a function of the distance from the white dwarf surface. The 'accretion curtain' model (see Rosen et al. 1991, and references therein) used to explain the behaviour of EX Hya, for instance, envisages an emission region that extends to $\sim 1 R_{\rm wd}$ above the surface, with the highest temperature emission occurring closest to the white dwarf.

(2) An inhomogeneous distribution of absorbing/scattering material above each polar cap. Studies of the X-ray spectra of intermediate polars have suggested that the X-ray continuum is seen through highly structured, or at least 'partial covering', absorbing material. This is one way, for instance,

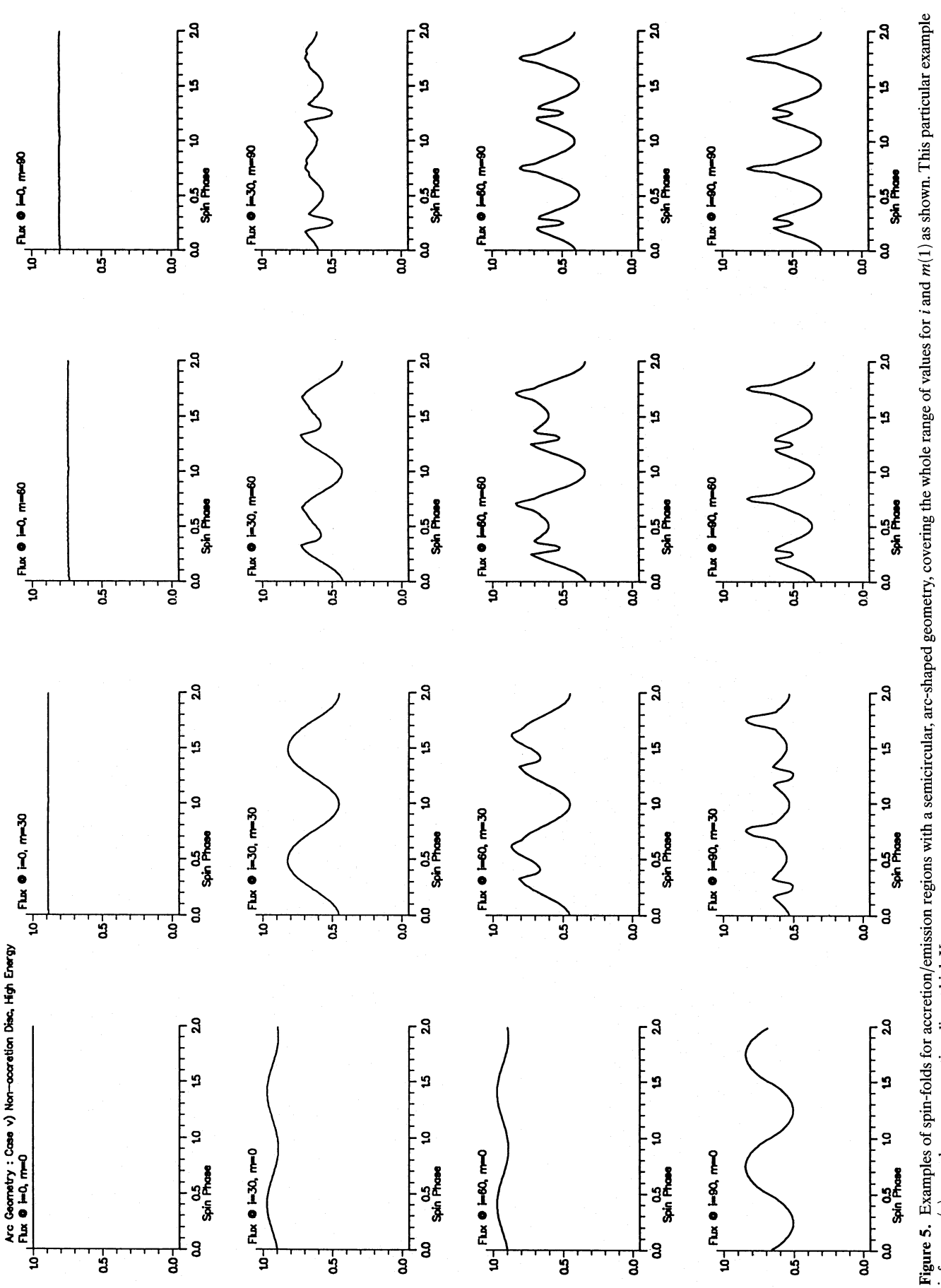

Figure 5. Examples of spin-folds for accretion/emission regions with a semicircular, arc-shaped geometry, covering the whole range of values for i and $m(1)$ as shown. This particular example is for case (v), namely a non-accretion disc at high X-ray energy.

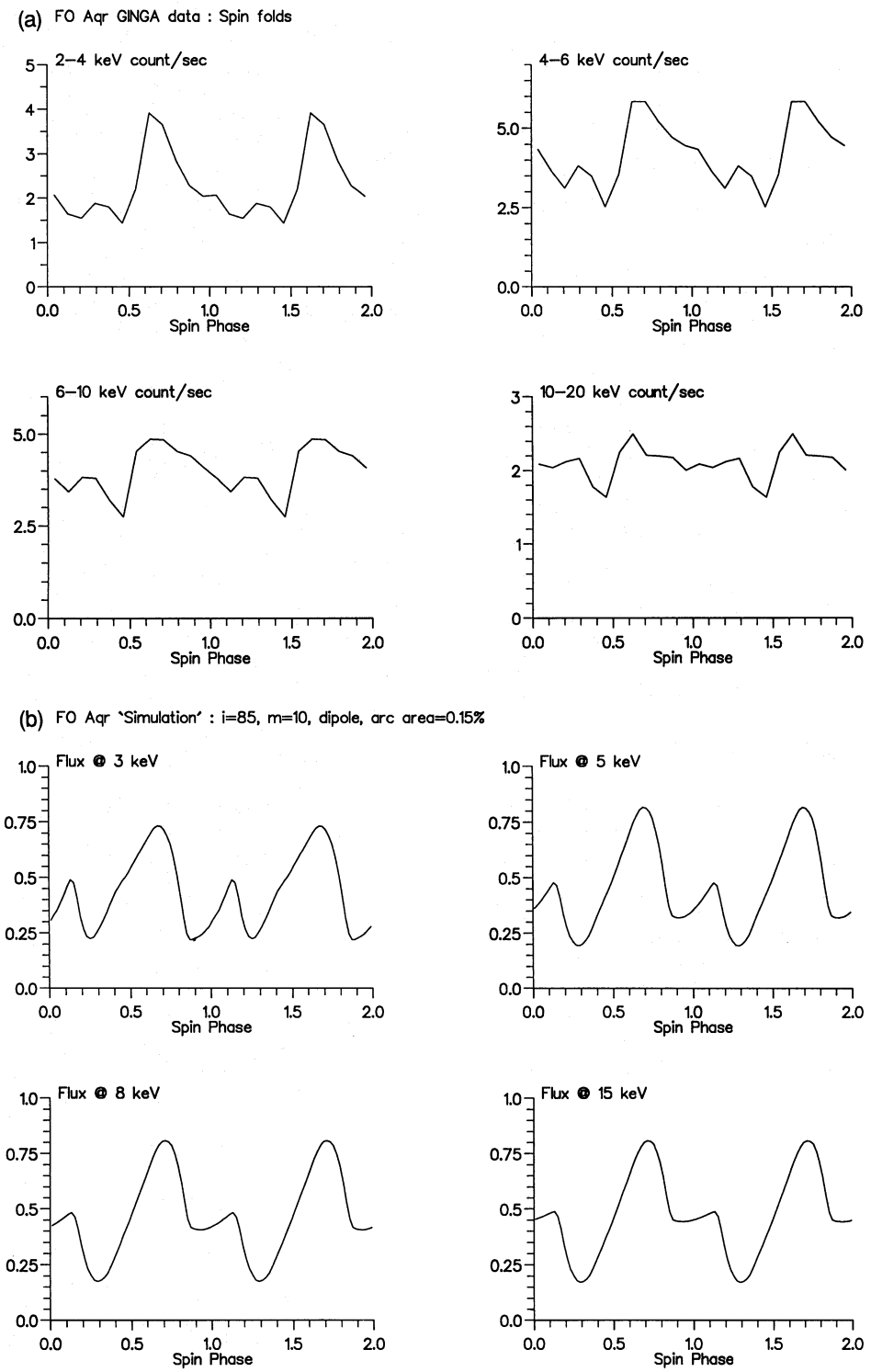

Figure 6. A comparison between (a) the *Ginga* spin-pulse profile data for FO Aqr and (b) the results of running the simulation code with the parameters $i = 85°$, $m(1) = 10°$, $m(2) = 190°$, $f(1) = f(2) = 0.01$, $f'(1) = f'(2) = 0.25$, $f''(1) = f''(2) = 0.3$, $\delta = 1.0$.

of explaining the anomalous strength of the iron Kα emission line which is seen in all intermediate polars (Norton, Watson & King 1991).

(3) Direct heating of the white dwarf surface, giving rise to a second X-ray component. It has been suggested that a large fraction of the accreting material in magnetic cataclysmic variables may be decelerated within the photosphere of the white dwarf itself, thus giving rise to a strong blackbody X-ray component (e.g. Hameury & King 1988). Such a component is generally not observed in intermediate polars, probably because the local column density is so high. However, the blackbody emission could in turn be reprocessed in

the material above the white dwarf surface, re-emerging elsewhere in the X-ray spectrum. The exact modulation that such a component would experience is unclear.

(4) The inclusion of random fluctuations in both the amount and trajectory of the accreting material. It has been assumed that the accreting material closely follows the magnetic field lines once it crosses the magnetosphere. In reality, the flow is likely to be far more chaotic than assumed here, and the influence that this will have on the temporal variation in X-ray emission has not been investigated.

In spite of these limitations of the present model, it is not clear that any of the effects mentioned above will cause dramatic differences in the light curves obtained. Hence a few general comments can be made with regard to the results.

When occultation, photoelectric absorption/electron scattering and the effects of accretion directly from the stream are all taken into account, simple circular geometries can produce spin-pulse profiles that are broadly similar to those observed, i.e. generally sinusoidal. Two important points to note are that this occurs *without* the assumption of any special conditions regarding the visibility or otherwise of one of the magnetic poles, and that even purely stream-fed models still give rise to strong modulation at the spin period. Also, as has previously been noted (e.g. Hellier 1991; King & Lasota 1991), purely disc-fed models cannot give rise to any form of beat modulation.

Perhaps the most important result to arise from these model light curves is that very complex pulse profiles (cf. Fig. 6b) can be produced from innately symmetric geometrical arrangements. These light curves bear a strong resemblance to those recently obtained by *Ginga* and *ROSAT*. The features necessary to produce these complexities are that the accretion/emission areas do not extend to all azimuthal angles around a given magnetic pole (e.g. arcs) and that some (at least) of the accretion flow is channelled directly via the stream. This gives rise to the 'migrating' polar cap effect, which is modelled here for the first time. This is a simple way of producing the notch or shoulder structures that are seen, and it is difficult to see how such an effect could be avoided in practice.

ACKNOWLEDGMENTS

The original version of the computer code was based on another 'light curve generation program' developed by John Brooker whilst he and the author were at Leicester University. The simulations presented here were run at Southampton University on the Starlink node, which is funded by the UK SERC, and at the Open University. Thanks are due to Ian McHardy and Andrew King for their constructive comments on earlier versions of this paper, and to various other magnetic CV enthusiasts for ongoing discussions and advice. Thanks are also due to Tony Gomm for drawing Fig. 1, and to the anonymous referee for suggesting a more thorough investigation of the FO Aqr 'model'.

REFERENCES

Hameury J. M., King A. R., 1988, MNRAS, 235, 433
Hameury J. M., King A. R., Lasota J. P., 1986, MNRAS, 218, 695
Hellier C., 1991, MNRAS, 251, 693
Hellier C., 1992, MNRAS, 258, 578
Hellier C., Mason K. O., Cropper M., 1989, MNRAS, 237, 39P
Hellier C., Garlick M. A., Mason K. O., 1993, MNRAS, 260, 299
Ishida M., 1991, PhD thesis, Univ. Tokyo (ISAS Research Note 505)
Ishida M., Sakao T., Makishima K., Watson M. G., Norton A. J., Kawada M., Koyama K., 1992, MNRAS, 254, 647
King A. R., Lasota J. P., 1991, ApJ, 378, 674
King A. R., Shaviv G., 1984, MNRAS, 211, 883
Mason K. O. et al., 1992, MNRAS, 258, 749
Nauenberg M., 1972, ApJ, 175, 417
Norton A. J., Watson M. G., 1989, MNRAS, 237, 853
Norton A. J., Watson M. G., King A. R., 1991, in Treves A., Perola G. C., Stella L., eds, Lecture Notes in Physics, Vol. 385, Iron Line Diagnostics in X-ray Sources. Springer-Verlag, Berlin, p. 155
Norton A. J., Watson M. G., King A. R., Lehto H. J., McHardy I. M., 1992a, MNRAS, 254, 705
Norton A. J., McHardy I. M., Lehto H. J., Watson M. G., 1992b, MNRAS, 258, 697
Rosen S. R., Mason K. O., Mukai K., Williams O. R., 1991, MNRAS, 249, 417
Wynn G. A., King A. R., 1992, MNRAS, 255, 83